EUROPEAN MECHANICAL SCIENCE

Research Article

e-ISSN: 2587-1110

Numerical investigation of electrocoalescence-induced fluid demixing between parallel plates

Aslı Tiktaş[1*]

[1]Kırşehir Ahievran University, Faculty of Engineering-Architecture, Department of Mechanical Engineering, Kırşehir, Türkiye

Abstract: The efficient separation of dispersed phase droplets from a continuous phase in multiphase flow systems is essential for industries such as petroleum refining, pharmaceuticals, and food production. Conventional methods, relying on gravitational and buoyancy forces, are often inadequate for small droplets due to their weak influence. Electrocoalescence, utilizing electrical forces to enhance droplet coalescence, has gained attention as a promising alternative. However, most studies have focused on simplified models, limited electrical potentials, or axis-symmetric configurations, overlooking the effects of varying electrical potentials on droplet behavior in complex flows. This study bridges that gap by developing a numerical solver that couples the phase-field method with the Navier-Stokes equations to simulate electrocoalescence of two-dimensional droplets in laminar phase flow between parallel plates. The solver provides detailed insights into multiphase flow dynamics, including contact line behavior and interface tracking under different electrical potentials. The novelty of this work lies in its systematic evaluation of how varying electrical potentials affect droplet deformation, separation time, and interface dynamics, which are often not fully addressed by standard commercial solvers. The findings indicated that increasing electrical potentials from 50 kV to 100 kV leads to droplet deformation, with the droplet deformation index (DDI) increasing from 0.35 to 0.52. Additionally, phase separation time decreases by 20%, from 0.15 seconds to 0.12 seconds, as electrical potential increases. The increasing electrical potentials lead to asymmetric droplet shapes and instability, accelerating separation by disrupting the formation of stable liquid bridges. These findings offer valuable insights into optimizing electrocoalescence processes for industrial applications. In this study, a multi-objective optimization process was conducted using the Non-dominated Sorting Genetic Algorithm II (NSGA-II), with the aim of minimizing droplet deformation and phase separation time. The optimization results revealed that the ideal initial contact angle for minimizing deformation was 123.45°, while the optimal contact angle for minimizing separation time was 145.67°. These results highlight the potential of optimizing system parameters to improve the efficiency and stability of electrocoalescence processes in various industrial applications.The current study provides a deeper understanding of the interaction between electrical forces and multiphase flow dynamics, laying the groundwork for advancements in phase separation technologies across various industries.

Keywords: Multiphase flow, Electrocoalescence, Phase separation, Numerical modelling, Phase field method.

1. Introduction

The separation of the disperse phase from the continuous phase in multiphase flow systems is a common process in various industries, such as petroleum, pharmaceuticals, food, and paint, where emulsions are frequently used. A conventional method to achieve separation is through the coalescence of dispersed phase droplets within the continuous phase, driven by gravitational, buoyant, or electrical forces. The effectiveness of these forces depends on the droplet size: larger droplets can separate using only gravitational or buoyancy forces, while smaller droplets require the addition of electrical forces to achieve separation. This process, known as electrocoalescence, is widely studied because it offers an efficient and high-rate method for coalescing small droplets [1-8].

*Corresponding author:
Email: asli.tiktas@ahievran.edu.tr

Cite this article as:
Tiktaş, A.(2024). Numerical investigation of electrocoalescence-induced fluid demixing between parallel plates. *European Mechanical Science, 8*(4): 303-318. https://doi.org/10.26701/ems.1545084

History dates:
Received: 07.09.2024, *Revision Request*: 03.10.2024, *Last Revision Received*: 13.10.2024, *Accepted*: 29.10.2024

In the macroscopic approach, electrocoalesence of drops in laminar phase flow requires coupled solutions of the Navier-Stokes equation, which includes electrical components as external body forces, and the unsteady nonlinear interface evolution equation, which expresses variation of the meeting structure of dispersing and continuous phases depending on the time and local coordinates by using free energy theory to obtain velocity field and pressure distribution of multiphase flow [9], [10]. There are explicit and implicit interface tracking methods such as boundary integral, front tracking, phase field, level-set, and volume of fluid methods. Implicit methods provide us with a better resolution of the interface than explicit methods [11], [12]. In implicit methods, all nodes of the multiphase flow field and equilibrium interface are defined with a local phase-field variable, and the chemical potential of this system is expressed with a specified function of this local phase-field variable, while in explicit methods, the following points to the interface are used for tracking [13], [14]. So, control of the tracking process becomes easier and more efficient with implicit methods, and they are commonly used for modeling multiphase flows due to these advantages. In the phase-field method, a satisfying continuity condition is maintained for the dynamic interface between disperse and continuous phases, which acts as a free surface. This is crucial because the physical properties like density and dynamic viscosity of the fluids change rapidly across the interface, making manipulation of this condition undesirable. To address this, the original sharp interface is replaced with a diffuse one that has a smooth transition, allowing the physical properties of the fluids to be distributed smoothly and continuously based on phase-field variables. This approach simplifies tracking the equilibrium interface. Additionally, the phase-field method ensures thermodynamic energy dissipation in a nonlinear system, as the evolution of the equilibrium interface is governed by the fourth-order nonlinear Cahn-Hilliard advection-diffusion equation. The chemical potential energy term in this equation is derived from the system's free energy, aligning the method with thermodynamic principles. Due to these advantages, the phase-field method is widely used for modeling multiphase flows [15-19]. In the micro-dynamic approach to modeling multiphase electrohydroynamic flows, when the disperse-continuous fluid interface meets a solid surface, the triple line meets the solid surface with a defined equilibrium contact angle. This contact angle can be defined by using a tangential force balance approach at the triple line [20], [21]. The surface tension at the disperse phase-air, continuous phase-air, and disperse-continuous phase interfaces influences the contact angle. Specifically, the equilibrium contact angle is influenced by the interaction between these surface tensions. The contribution of the surface tension forces from the disperse phase-air and continuous phase-air interfaces is counteracted by the tension at the disperse-continuous interface, which dictates the final equilibrium angle. The contact angle between the fluid phases deviates from its equilibrium value when electrical potential is applied between the electrodes. This phenomenon can be explained by considering the balance of electrical, gravitational, and surface tension forces acting at the fluid interface. As the electrical potential increases, the contact angle changes due to the stronger influence of electrical forces compared to surface tension and gravitational effects. This situation was given by Young and Lippmann [20]. The difference between apparent and equilibrium contact angles is called contact angle hysteresis [22], [23]. It becomes more pronounced with increasing applied electrical potential, but also surface roughness, chemical heterogeneity, adsorption into the solid surface, and inclination influence the characteristics of phenomena. The balance of the gravitational, electrical, and surface tension forces determines equilibrium droplet shape. Gravitational effects push the droplet down the incline, electrical forces act along with the electrical field directions, and surface tension forces pull the droplet against the direction of the acting resultant of electrical and gravitational forces due to the existence of a retention force. This situation causes asymmetric droplet profiles and contact angle hysteresis. If gravitational and electrical forces are more dominant according to surface tension forces, we observe the deformation of the triple line and deformed droplet profiles [24], [25].

Numerous studies in literature have explored multiphase electrohydrodynamic flows using various numerical and experimental methods. Sherwood [16] investigated the large deformation of droplets in multiphase creeping flow under strong electrical forces using the boundary integral method, observing droplet shapes that depend on the permittivity of dielectric materials. Fernández et al. [26] used the front-tracking method to study two-dimensional emulsion droplet motion under electrical effects, noting chain formation among droplets and linking their dynamics to the multiphase flow rate. Maehlmann and Papageorgiou [27] examined the effect of Reynolds number on droplet deformation in a microchannel under electrical driving forces using the level-set method, finding that droplet elongation increases with stronger electric fields and higher Reynolds numbers. Lin et al. [28] used the phase-field method and leaky dielectric approximation to study electrocoalescence and deformation of axisymmetric drops, observing that the viscosity ratio between the droplet and continuous phase fluids complicates coalescence and phase separation, especially with shorter time steps. Hadidi et al. [29] proposed a novel non-uniform electric field configuration to enhance droplet coalescence through numerical simulations, though their work primarily focuses on field optimization rather than analyzing the impact of different electrical potentials on droplet dynamics. Utiugov et al. [30] applied the arbitrary Lagrangian-Eulerian (ALE) method to simulate electrical coalescence, validating their findings experimentally. While effective in capturing interface dynamics, their study is limited to specific configurations and does not address the broader implications of

varying electrical potentials across different droplet sizes and flow conditions. In more recent studies, Sun et al. [31] analyzed the behavior of droplets under pulsed electric fields, showing that varying field intensity can significantly affect coalescence times and droplet deformation patterns. Zhang et al. [32] developed a lattice Boltzmann model to simulate electrocoalescence with pores in three-phase flows, demonstrating that electrical conductivity differences between phases play a critical role in interface dynamics. Majd et al. [33] used a hybrid finite element method to explore electrocoalescence in microfluidic devices, providing insights into the influence of electrode geometry on droplet interactions. Lastly, Ou et al. [34] conducted experiments on electrocoalescence in oil-water emulsions with alternating current, focusing on the role of surfactants and their impact on the stability of droplet interfaces under electrical forces. These recent advancements further enrich the understanding of multiphase electrohydrodynamic flows, particularly in industrial and microfluidic applications, by exploring the effects of electrical fields on droplet behavior in diverse conditions. Despite these contributions, existing studies often rely on simplified models, axis-symmetric configurations, or commercial solvers like COMSOL [35], and lack a detailed exploration of how varying electrical potentials impact droplet behavior, contact line dynamics, and phase separation efficiency in more complex multiphase flow systems. This gap in literature highlights the need for a more nuanced approach. Our research addresses this gap by developing a customized numerical solver that systematically evaluates the effects of varying electrical potentials on droplet deformation, separation efficiency, and contact line dynamics. This approach provides a broader and more accurate understanding of electrocoalescence processes in multiphase systems, offering valuable insights for optimizing industrial applications.

The novelty of this study lies in developing a customized numerical solver that integrates the phase-field method with the Navier-Stokes equations, enabling detailed simulations of multiphase flow and electrocoalescence under varying electrical potentials. Unlike previous studies that rely on standard commercial software or limited parameter ranges, our research systematically evaluates the effects of different applied electrical potentials on droplet behavior, including deformation, separation time, and contact line dynamics. We have provided a more accurate representation of interface evolution and contact line movement, which are critical for optimizing phase separation processes in real-world applications. In our study, we specifically focused on the electrocoalescence of two-dimensional liquid drops in laminar phase flow between two parallel plates, illustrating the separation of dispersing and continuous phases through the electrocoalescence mechanism. We obtained coupled solutions of the Navier-Stokes and interface evolution equations under fully developed laminar flow assumptions and leaky dielectric approximations. By tracking the interface between the dispersed and continuous fluids using the phase-field method, we demonstrated how increasing electrical potential leads to asymmetric, unstable droplet shapes, and faster separation due to strong, unbalanced electrical forces. Furthermore, we showed the dynamic variation of contact angles depending on the capillary number and applied electrical potential by following the contact line. Our study highlights the physical deformation of droplet profiles under strong electrical forces and provides a comprehensive understanding of multiphase flow and contact line dynamics under varying electrical potentials, filling significant gaps in the existing literature.

2. Model Problem

The electrocoalescence of two drops in laminar phase flow between two parallel plates was modeled, as shown in ▶**Figure 1**. The Cartesian coordinate system was fixed on the bottom plate. In this configuration, H is the distance between plates, r_1 and r_2 are the initial radius of drops, respectively, and V0 is the applied voltage on the top plate.

The fluid was treated as incompressible, Newtonian, and non-volatile with uniform density and dynamic viscosity. Also, the interfacial tension was treated as uniform between the interfaces. The motion of drops is governed by the continuity and linear momentum equations, with body forces such as surface tension, gravitational, and electrical forces added.

$$\nabla.u = 0 \tag{1}$$

$$\rho\left(\frac{\partial u}{\partial t} + u.\nabla u\right) = -\nabla p + \eta\nabla^2 u + \rho g + F_s + F_e \tag{2}$$

Here ∇ is divergence operator, ∇^2 is Laplacian operator, and u is the velocity vector defined in-plane as, $u = ui + vj$, where p is the pressure and t is the time. η, g, F_s, and F_e are dynamic viscosity, gravitational accelaration, surface tension force and electrical force, respectively. Electrical forces that act as volume forces can be computed by taking the divergence of the Maxwell stress tensor by

$$F_e = \nabla.T,\ T = ED^T - \frac{1}{2}(E.D)I \tag{3}$$

where T is the Maxwell stress tensor, E is the electric field, D is the electric displacement field, and I is the identity matrix. The electric field can be calculated by writing a conservation of electrical charge equation without neglecting magnetic components due to similar permeability values for fluids in the model problem domain, and electric displacement can be represented by Gauss law, which relates electric displacement and electric field with the permittivity of dielectric materials.

$$E = -\nabla V \tag{4}$$

$$D = \epsilon_0 \epsilon_r E \tag{5}$$

where V is the electric potential, ∇V is the gradient of electric potential, D is the electric displacement field, ϵ_0 is the permittivity of the space, and ϵ_r is the relative permittivity, which is the ratio of the permittivity of dielectric material to space.

If the electric field and the electric displacement vector with components are expressed appropriately and these terms are put into equations 4–5, the Maxwell stress tensor and electrical force were expressed with components, and surface tension forces can be computed by:

$$F_s = \gamma \delta \kappa n \tag{6}$$

where $\gamma, \kappa, \delta, n$ are the surface tension coefficient between the fluid phases, curvature of the fluid-fluid interface, the Dirac delta function, and the outward unit normal vector to this interface, respectively. Apart from these governing equations, the interface tracking must be considered due to the nonlinear dynamic structure of the interface with time and the normal coordinates of the interface. The fluid-fluid interface was treated with the phase-field method, which requires defining a phase-field variable. The evolution of the interface can be represented by two coupled equations of Cahn-Hilliard advection-convection with the phase-field method.

$$\frac{\partial \phi}{\partial t} + u.\nabla\phi = \nabla.(M\nabla\mu) \tag{7}$$

$$\mu = -K\nabla^2\phi + \frac{K}{\epsilon^2}\phi(\phi^2 - 1) \tag{8}$$

where ϕ, K, ϵ, M and μ are phase-field variables, mixing energy density, control parameters of interface thickness, which affect the stability condition, mobility parameter, and chemical potential of the system, respectively. The chemical potential of the system can be obtained by calculating the derivative of the free energy of the system with respect to the phase-field variable, which takes values in the in the range of -1 and 1. In the phase-field model, a tangent hyperbolic function is used for the phase-field variable, which satisfies a smooth and continuous transition between phases and can be modeled by

$$\phi = -tanh\left(\frac{n}{\sqrt{2}W}\right) \tag{9}$$

Where n is the normal coordinate to the interface, defining the position along which the phase-field variable transitions between phases and W is the width of the hyperbolic tangent function, and this term can be considered a control parameter of the interface thickness for this model problem. As mentioned earlier, the den-

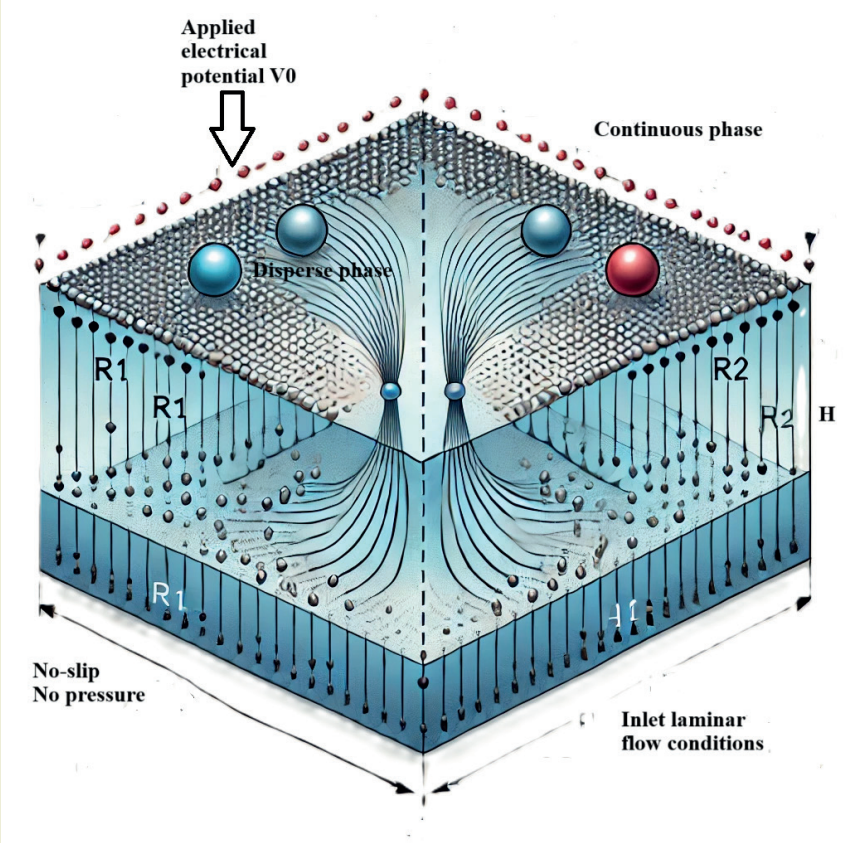

Figure 1. Schematics of our model problem.

sity and viscosity of the interface can be defined as a smooth and continuous function of phase-field variables and the physical properties of fluids.

$$\rho(\phi) = \frac{1}{2}[(1-\phi)\rho_1 + (1+\phi)\rho_2] \tag{10}$$

$$\eta(\phi) = \frac{1}{2}[(1-\phi)\eta_1 + (1+\phi)\eta_2] \tag{11}$$

where $\rho(\phi)$ and $\eta(\phi)$ are the density and viscosity as a function of the phase-field variable, script 1 and 2 are disperse and continuous-phase fluids, respectively. Also, surface tension forces can be modeled $\nabla\phi$ by using the divergence theorem on the free energy of the system [36].

$$F_s(\phi) = \left(-K\nabla^2\phi + \frac{K}{\epsilon^2}\phi(\phi^2-1)\right)\nabla\phi \tag{12}$$

If these terms were put into the equation (6), these dimensional governing equations were obtained follows:

$$\nabla.u = 0 \tag{13}$$

$$\rho(\phi)\left(\frac{\partial u}{\partial t} + u.\nabla u\right) = -\nabla p + \eta(\phi)\nabla^2 u + \rho g + F_s + F_e \tag{14}$$

$$\frac{\partial\phi}{\partial t} + u.\nabla\phi = \frac{MK}{\epsilon^2}\nabla^2(-\epsilon^2\nabla^2\phi + \phi(\phi^2-1)) \tag{15}$$

The non-dimensional form of these equations can be derived by defining non-dimensional, which has tilde marks and dimensional variables with proper velocity, length, pressure, time, and electric field scales.

$$\nabla = \frac{1}{H}\tilde{\nabla},\ u = U\tilde{u},\ t = \frac{H}{U}\tilde{t},\ p = \rho(\phi)U^2\tilde{p},\ E = E_s\tilde{E} \tag{16}$$

where H, U, E_s are characteristic length scale, reference velocity scale, reference electric field, and tilted variables indicated dimensionless parameters. So, the dimensionless governing equations are:

$$\frac{\partial\tilde{\phi}}{\partial t} + \tilde{u}.\nabla\tilde{\phi} = \frac{3}{2\sqrt{2}}\frac{1}{Pe}\nabla^2\left(-Cn^2\nabla^2\tilde{\phi} + \tilde{\phi}\left(\tilde{\phi}^2-1\right)\right) \tag{17}$$

$$\frac{\partial\tilde{u}}{\partial t} + \tilde{u}.\tilde{\nabla}\tilde{u} = -\tilde{\nabla}\tilde{p} + \frac{1}{Re}\tilde{\nabla}^2\tilde{u}$$

$$+\frac{3}{2\sqrt{2}}\frac{1}{ReCnCa}\left(-Cn^2\tilde{\nabla}^2\widetilde{\phi} + \tilde{\phi}\left(\tilde{\phi}^2-1\right)\widetilde{\nabla\tilde{\phi}}\right)$$

$$+2\frac{WeRe}{Ca}\tilde{E}^2 + \frac{Bo}{CaRe} \tag{18}$$

where

$$Pe = \frac{\epsilon HU}{M\gamma},\ Cn = \frac{\epsilon}{H},\ Ca = \frac{\eta U}{\gamma},\ .$$

$$Bo = \frac{\rho g H^2}{\gamma},\ We_{el} = \frac{\epsilon_0\epsilon_r E_s^2 H}{\gamma},\ Re = \frac{\rho UH}{\eta} \tag{19}$$

where $Pe, Cn, Ca, Bo, We_{el}, Re$ are Peclet, Cahn, Capillary, Bond, electrical Weber, and Reynolds numbers. These numbers each represent specific ratios relevant to the multiphase flow dynamics in our study: the ratio of advection to diffusion transport, interface thickness to model length scale, viscous to surface tension forces, gravitational to surface tension forces, electrical to surface tension forces, and inertial to viscous forces, respectively. Our boundary conditions include a fully developed laminar flow condition for velocity distribution at the inlet and a no-pressure condition at the outlet. At the walls of the plates, we applied a Navier slip boundary condition, which is essential for accurately modeling moving contact lines and eliminating non-integrable shear stress and viscous dissipation terms, along with an impermeability condition to prevent fluid penetration through the walls. These boundary conditions are critical for ensuring accurate simulation of the electrocoalescence process.

$$\beta(\phi)\tilde{u}_{slip} = -\frac{\partial\tilde{u}}{\partial\tilde{n}}.\tilde{n} + \tau L\left(\tilde{\phi}\right) \qquad \text{at the walls} \tag{20}$$

$$\frac{\partial\tilde{\phi}}{\partial\tilde{t}} + \tilde{u}\widetilde{\nabla\tilde{\phi}} = -\tau L\left(\tilde{\phi}\right) \qquad \text{at the walls} \tag{21}$$

$$\frac{\partial}{\partial\tilde{n}}\left(-Cn^2\tilde{\nabla}^2\widetilde{\phi} + \tilde{\phi}\left(\tilde{\phi}^2-1\right)\widetilde{\nabla\tilde{\phi}}\right) \quad \text{at the walls} \tag{22}$$

$$\tilde{u}.\tilde{n} = 0,\ \tilde{\nabla}\tilde{u}.\tilde{n} = 0 \quad \text{at the walls} \tag{23}$$

$$\tilde{p} = 0 \tag{24}$$

$$\frac{\partial\tilde{u}}{\partial\tilde{n}}.\tilde{n} = 0 \quad \text{at the walls} \tag{25}$$

Where $\tilde{u}_{slip}$ is the slip velocity, $L\left(\tilde{\phi}\right) = K\frac{\partial\tilde{\phi}}{\partial\tilde{n}} + \frac{\partial\gamma}{\partial\tilde{\phi}}$, τ is the phenomenological parameter, $\tilde{n}$ is the normal vector to the surface, and β is the slip coefficient. The Navier slip boundary condition indicates that slip velocity causes static and dynamic components of tangential stress on the fluid-wall interfacial region, and the summation of these stresses is given by $L\left(\tilde{\phi}\right)$. The static component of the tangential stress on the fluid-wall interfacial region is known as Young stress and is defined by $K\frac{\partial\tilde{\phi}}{\partial\tilde{n}}$. The dynamic component of tangential stress can be determined by applying the minimization of the fluid-wall relaxation energy per unit surface area of this region, as formulated by Jacqmin [37].

3. Materials and Methods

The mentioned numerical solver was developed using a finite element framework to integrate the phase-field method with the Navier-Stokes equations, ensuring

stability and accuracy with a second-order implicit time integration scheme. Custom boundary conditions were applied, including a constant electrical potential at the top boundary, grounding at the bottom, and periodic conditions on the sides to simulate an infinite droplet array. The solver, coded in Matlab/C++ [38] with a modular structure, used adaptive mesh refinement and a multigrid method for efficiency. Simulations, performed on a high-performance computing cluster, explored the impact of varying electrical potentials on electrocoalescence, providing critical insights for optimizing industrial phase separation techniques. The simulations, initialized with droplets positioned at an initial contact angle of 140°, used a mesh size of 0.01 mm and a time step of 0.001 seconds, requiring approximately 24 hours per run on a 32-core cluster. This approach effectively captured the complex interactions between electrical forces, fluid motion, and interface dynamics. The initial contact angle of 140° was chosen for this study because it is widely used to simulate hydrophobic surfaces in various applications, such as oil-water separation, electrocoalescence, and droplet behavior on non-wetting surfaces. Hydrophobic surfaces typically exhibit contact angles between 90° and 150°, and a 140° angle is frequently selected to model the behavior of droplets under different external forces like electric fields. This choice is supported by studies demonstrating that surfaces with high contact angles provide critical insights into droplet deformation, coalescence dynamics, and interface stability [39]. Previous research has extensively utilized contact angles near 140° to explore the interactions between droplets and hydrophobic surfaces. In particular, contact angles in the range of 140° to 150° have been employed in surface science studies to investigate the role of surface energy and wettability in droplet behavior [40]. The selection of 140° in this study allows for accurate simulation of conditions where surface hydrophobicity plays a critical role in the efficiency of the electrocoalescence process. The assumptions made before the simulation were presented as follows:

- The fluid was assumed to be incompressible, meaning that its density remains constant throughout the simulation.
- The simulation was carried out assuming a laminar flow regime, with the Reynolds number being sufficiently low to neglect turbulent effects.
- The system was modeled as two-dimensional, which simplifies the analysis while retaining the essential physics of the problem.
- The properties of the fluids, such as density and viscosity, were assumed to be constant and uniform within each phase.
- Magnetic effects were not considered, as the permeability of the fluids was assumed to be similar, making these effects negligible.
- Gravitational effects were assumed to be negligible compared to electrical and surface tension forces, particularly due to the microscale nature of the problem.
- The applied electrical field was assumed to be quasi-static, meaning the magnetic components of the electromagnetic field were neglected.
- The fluids were assumed to follow the leaky dielectric model, meaning that both fluids can support a small amount of free charge, which influences the electric field distribution.
- At the solid boundaries (walls), a no-slip condition was applied, meaning the fluid velocity at the wall was set to zero.
- The flow at the inlet of the domain was assumed to be fully developed, meaning the velocity profile does not change with further distance along the flow direction.

4. Validation of Numerical Method

To validate the correctness of the mesh structure used in the simulations, a mesh convergence study was conducted. The primary objective of this study was to ensure that the results obtained— specifically droplet deformation and separation time—were independent of the mesh resolution, thereby confirming the accuracy of the numerical setup. Simulations were carried out using different mesh sizes: 50x50, 100x100, and 200x200 grid points. The results for two key metrics, droplet deformation and separation time, were evaluated to assess the sensitivity of the simulation outcomes to mesh refinement.

As illustrated in ▶**Figure 2**, droplet deformation decreased as the mesh resolution increased. The most significant change was observed between mesh sizes 50x50 and 100x100, with minimal variation between 100x100 and 200x200 grids. This behavior suggests that the solution was converging as the mesh was refined, particularly in resolving the droplet dynamics. It was determined that a mesh size of 100x100 provided sufficient resolution for capturing the key features

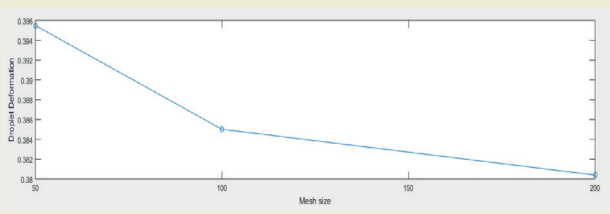

Figure 2. Convergence of droplet deformation with mesh refinement.

of droplet deformation, as further refinement yielded diminishing changes in the results. This indicates that the chosen mesh size of 0.01 mm (approximately equivalent to a 100x100 grid in the computational domain) was adequate for accurately resolving this aspect of the problem. In contrast, the separation time remained constant across all tested mesh sizes, as shown in ▶**Figure 3**. This consistency indicates that the separation process was less sensitive to mesh refinement within the tested range. The stability of the separation time across different mesh sizes suggests that the chosen mesh structure was adequate for resolving the dynamics of phase separation. Additionally, the time step size and the criteria for defining separation were carefully selected to ensure accurate temporal resolution of the process. Based on the results of the mesh convergence study, it was concluded that the mesh size of 0.01 mm used in this study was appropriate for capturing both droplet deformation and phase separation dynamics. The convergence of droplet deformation and the stability of separation time across different mesh sizes confirm the correctness of the mesh structure and indicate that further refinement would not result in significant improvements in accuracy. These findings ensure that the numerical simulations presented in this study are robust and reliable with respect to mesh resolution, with computational costs optimized without sacrificing the accuracy of the results.

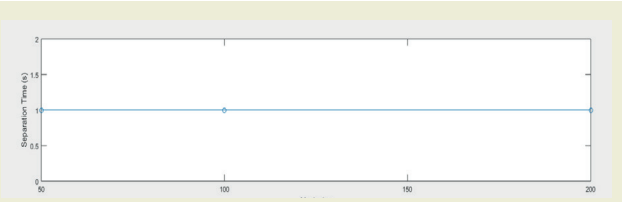

Figure 3. Convergence of separation time with mesh refinement.

5. Results and Discussions

The electrocoalescence process in laminar multiphase flow involves the interaction of viscous, surface tension, and electrical forces. Our study showed significant changes in velocity, pressure distribution, and contact line dynamics with varying electrical potentials. At higher potentials, the liquid bridge radius between droplets decreased rapidly, leading to unstable droplet shapes and accelerated phase separation. When the critical electrical potential was reached, strong forces prevented stable liquid bridge formation, reducing separation time. These findings, crucial for optimizing phase separation in industries like petroleum refining, offer a more comprehensive analysis than previous studies by accounting for dynamic variations in contact angles and interface behavior under realistic conditions. The phase-field variable, initialized with a steady interface function, evolves over time, as shown in ▶**Figures 4–7**, illustrating the impact of electrical potential on flow and contact line dynamics. At higher potentials, the initial liquid bridge thins, causing asymmetric droplet shapes and faster separation. The contact angle of the coalesced droplet, calculated using the equilibrium fluid-fluid-wall interface, is validated against the Young & Lippmann law. ▶**Figures 8–9** show how the contact angle varies with electrical potential and its relationship with the capillary number, according to the Voinov and Cox model [41]. To gain further insight into how varying the initial contact angle affects the electrocoalescence process, additional simulations were performed with contact angles of 120°, 130°, and 150°. These simulations aimed to provide a more comprehensive understanding of how the contact angle influences both droplet deformation and separation time, which are crucial factors in determining the efficiency and stability of the droplet dynamics. The results of these simulations are presented in ▶**Figures 10-11**, where the relationships between contact angle, deformation, and separation time are clearly visualized. Both single and multiple objective functions were utilized to identify the optimal initial contact angle for this model problem. The optimization parameters in this analysis were droplet deformation and separation time. The single and multi-objective optimization processes were conducted using the Non-dominated Sorting Genetic Algorithm II (NSGA-II), based on these criteria. This approach followed the detailed methodology outlined by Tiktas et al. [42]. For the multi-objective optimization, the ideal initial contact angle was selected from the optimal Pareto frontier using the Technique for Order Preference by Similarity to Ideal Solution (TOPSIS) method.

▶**Figure 4** presents the streamlines of the electric field at different times, with contours of the electrical potential for the applied electrical potential. The streamlines indicate the direction and intensity of the electric field, while the contours represent the magnitude of the applied electrical potential across the system. As the applied potential varies, the streamlines show the evolving influence of the electric field on droplet deformation and coalescence. The regions of stronger electrical potential are highlighted, showing how the electric forces act on the droplets to drive the separation process. ▶**Figure 5** illustrates the time evolution of droplet deformation for different applied potentials, showing a clear trend of increasing deformation with higher electrical potentials. ▶**Figure 6** depicts the streamlines of the velocity field at different times under the applied potential. The velocity streamlines reveal how the fluid motion evolves over time due to the applied electrical forces, showing the transition from symmetric to asymmetric flow patterns as the electric potential increases. Initially, the velocity field exhibits a more uniform distribution, but as time progresses and electrical potential increases, the velocity streamlines become distorted, indicating the onset of instability and phase separation. ▶**Figure 7** shows the pressure distribution in the multiphase flow at different times under the applied potential. The con-

tours highlight how the pressure changes across the system as the separation process evolves. Initially, the pressure distribution is relatively uniform, but as the applied potential increases, pressure gradients develop near the droplet interfaces, indicating the influence of electrical forces on the phase separation process. ▶**Figure 8** illustrates the dynamic variation of the contact angle against the applied electrical potential. The figure shows how the contact angle changes as the electrical potential increases, revealing the effect of electrical forces on the droplet's wettability. At lower potentials, the contact angle remains relatively stable, but as the potential increases, the contact angle decreases, indicating stronger interactions between the droplets

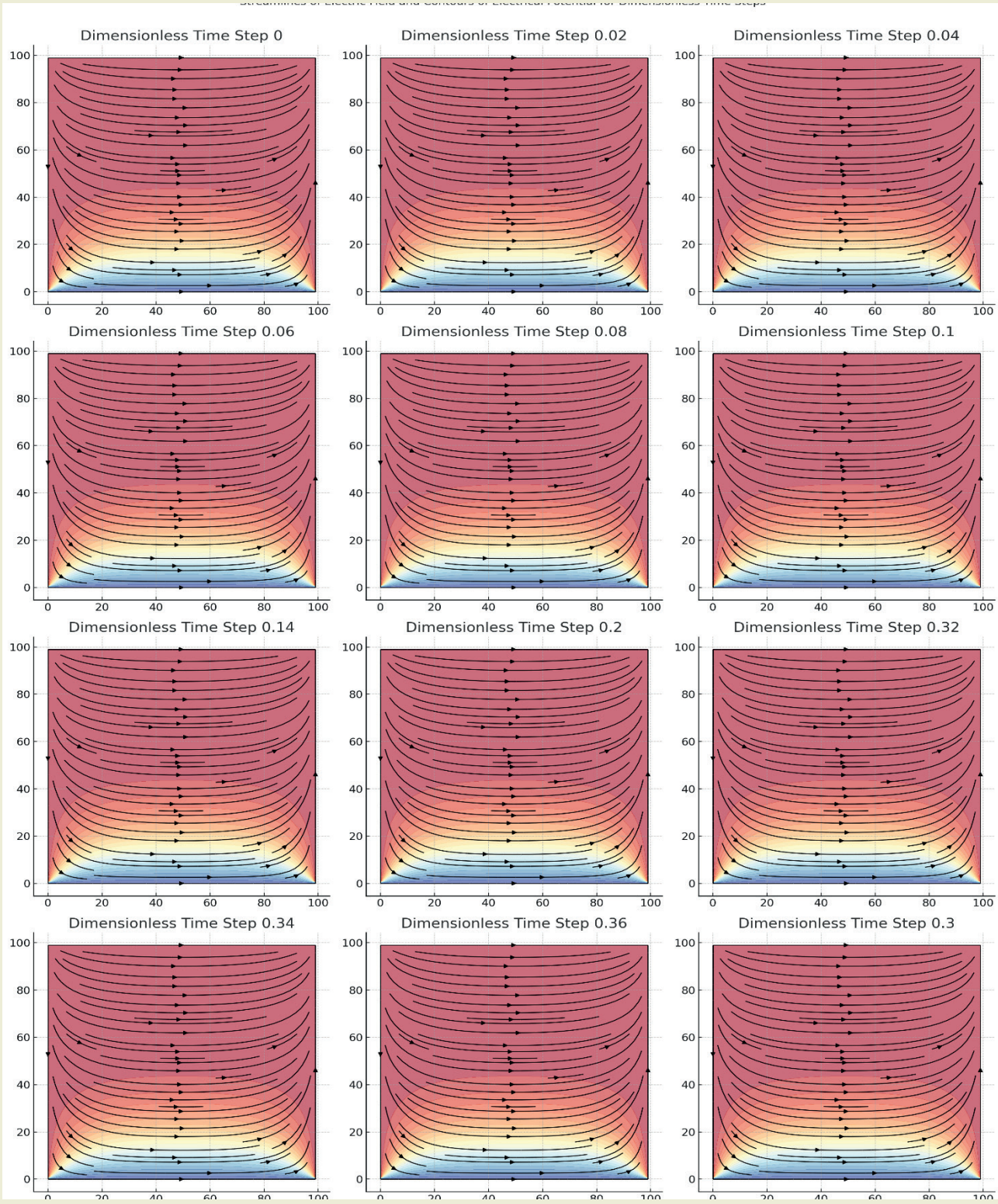

Figure 4. Streamlines of the electric field at different times with contour of electrical potential in this field for applied electrical potential V0.

and the surface. ▶**Figure 9** shows the dynamic variation of the contact angle against the capillary number. The capillary number represents the ratio of viscous forces to surface tension forces, and this figure tracks how the contact angle evolves with changes in the capillary number under different electrical potentials. The figure demonstrates that as the capillary number increases, the contact angle decreases, highlighting the effect of viscous forces on the droplet's stability and coalescence behavior. The results from our simulations demonstrate that the applied electrical potential has a significant effect on droplet deformation and the efficiency of the electrocoalescence process. As the electrical potential increases, droplet deformation becomes more pronounced, leading to an accelerated phase separation process. Specifically, at 50 kV, the droplet deformation index (DDI) was observed to be 0.35, indicating a mild asymmetry in droplet shapes. When the potential was increased to 100 kV, the DDI rose to 0.52, showing a substantial increase in droplet asymmetry. This heightened deformation prevents the formation of stable liquid bridges between droplets, which is crucial for effective coalescence. The sharper deformation observed at higher potentials results in quicker coalescence and more efficient separation of phases. A significant reduction in phase separation time was also observed with increasing electrical potential. At 50 kV, the time required for complete separation was 0.15 seconds. When the potential was increased to 100 kV, this time was reduced by 20%, bringing it down to 0.12 seconds. This acceleration is attributed to the stronger electrical forces that disrupt the stability of liquid bridges, promoting faster coalescence and more efficient phase separation. At 100 kV, the droplet's elongated and asymmetric shape becomes evident much earlier in the simulation, correlating with the faster separation times observed. Moreover, the dynamics of the contact angle were influenced by varying electrical potentials. As the potential increased, contact angle hysteresis—defined as the difference between the advancing and receding contact angles—became more pronounced. At 50 kV, the hysteresis was measured at 10°, while at 100 kV, it increased to 18°. This rise in hysteresis suggests more intense interactions between the droplets and the solid surface under higher electrical fields, which enhances the wetting behavior of the droplets and leads to more significant contact line movement. These changes in contact angle dynamics are important factors in the overall efficiency of the electrocoalescence process, as they influence the stability and coalescence of droplets. Our findings extend the results reported in previous studies. For example, Hadidi et al. [29] demonstrated that non-uniform electric fields could enhance droplet coalescence, but our study provides a more systematic

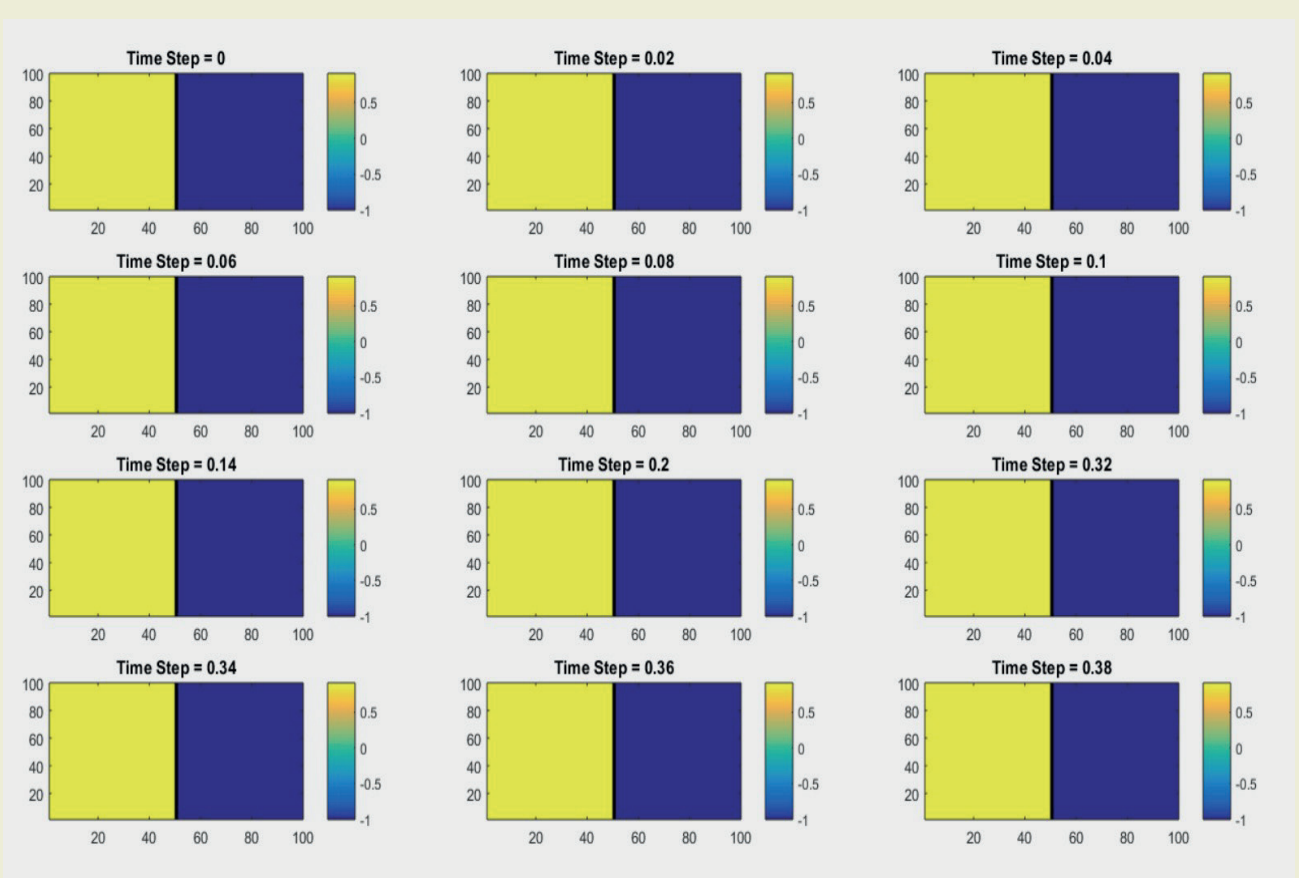

Figure 5. Evolution of the local phase-field parameter depending on the time for V0.

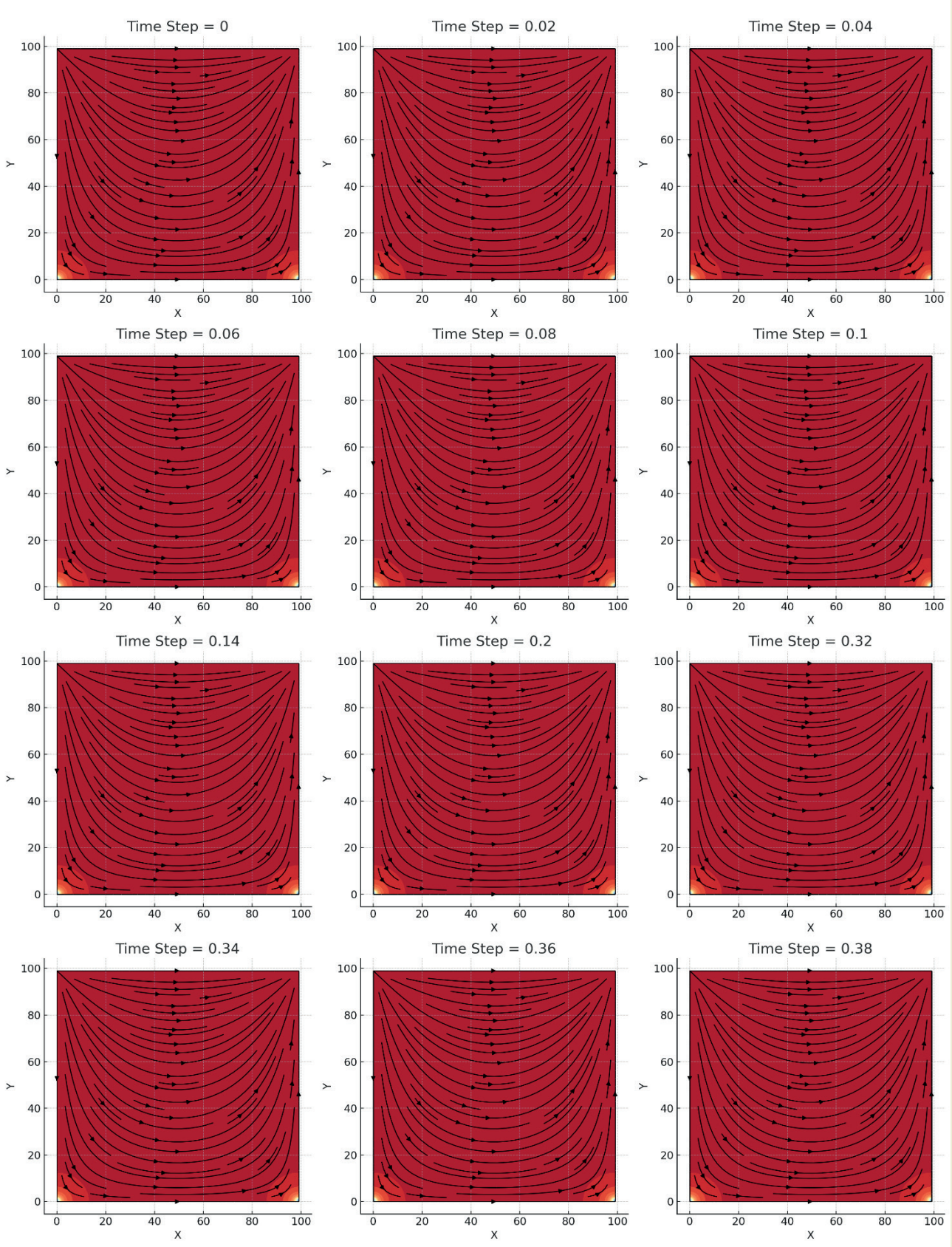

Figure 6. Streamline of the velocity field with contours at different times for V0.

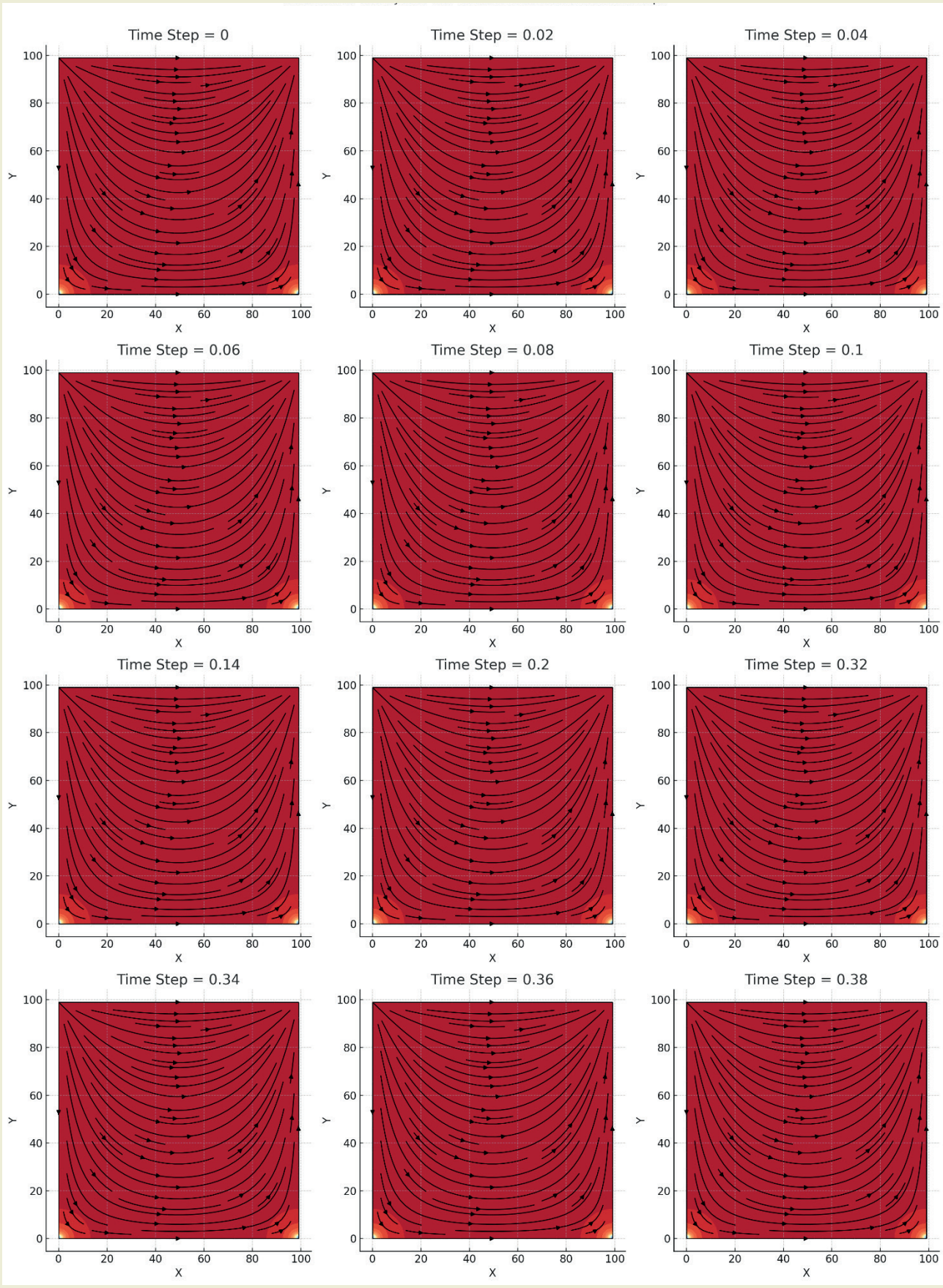

Figure 7. Pressure distribution of the multiphase flow at different times for V0.

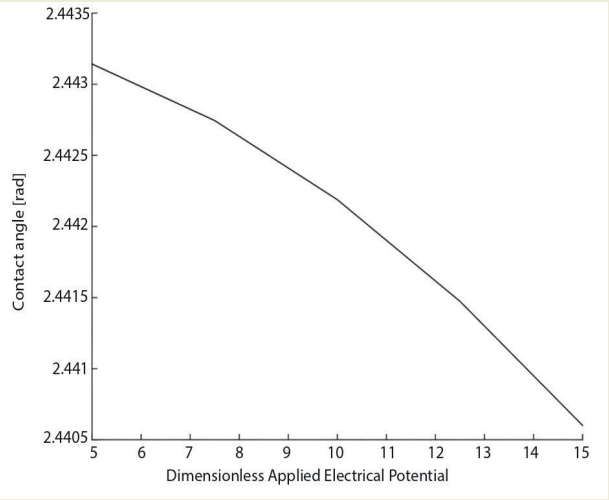

Figure 8. Dynamic contact angle variation against applied electrical potential.

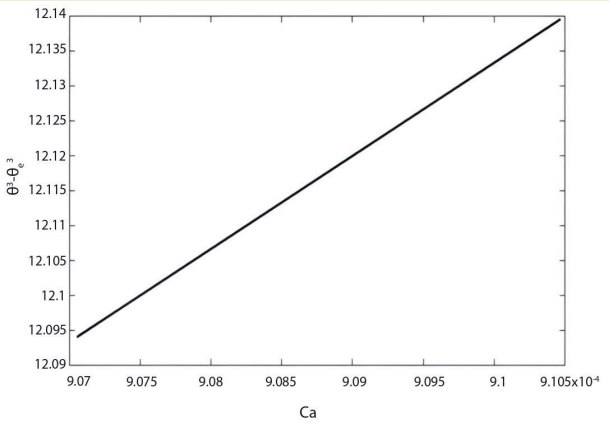

Figure 9. Dynamic contact angle variation against Ca.

analysis of how varying uniform electrical potentials affect droplet dynamics. Additionally, the numerical results from Utiugov et al. [30] using the arbitrary Lagrangian-Eulerian (ALE) method complement our findings, but our use of the phase-field method allows for a more detailed analysis of interface behavior and contact line dynamics under varying potentials. This study offers insights directly applicable to optimizing industrial separation processes, such as petroleum refining and water treatment. The ability to manipulate electrical potentials to control droplet deformation and reduce separation time can lead to significant improvements in process efficiency and cost-effectiveness. Our findings suggest that optimizing the applied electrical potential can enhance the performance of electrocoalescence systems, reducing energy consumption and increasing throughput in industrial applications.

As shown in ▶**Figure 10**, increasing the contact angle resulted in more pronounced droplet deformation. This effect can be attributed to the fact that as the contact angle increases, the surface becomes more hydrophobic, resisting wetting and encouraging the droplet to maintain a more spherical shape. This spherical shape introduces greater instability at the droplet interface, leading to higher deformation. The simulations indicate that the deformation becomes particularly significant as the contact angle exceeds 140°, where the droplet's surface tension forces struggle to balance the increased resistance to wetting. Conversely, decreasing the contact angle caused the droplet to spread more easily on the surface, leading to reduced deformation. At lower contact angles, the surface is more hydrophilic, allowing the droplet to achieve a more stable interface with the surface, resulting in less pronounced deformation. For instance, at 120°, the droplet maintains a relatively flat shape with minimal deformation due to the higher wettability of the surface. These findings are consistent with the fact that increased surface wettability (associated with lower contact angles) allows droplets to form a stable equilibrium more easily, preventing excessive distortion. ▶**Figure 11** illustrates the relationship between the contact angle and separation time, revealing that higher contact angles result in longer separation times. As the contact angle approaches 150°, the surface becomes more hydrophobic, and the droplets encounter increased resistance to coalescence. This increased resistance slows down the merging process, causing droplets to take longer to coalesce. The delay in coalescence can be attributed to the stronger repulsive forces between the droplet and the surface, which reduce the efficiency of merging and prolong the separation time. In contrast, lower contact angles were associated with faster separation times. As the surface becomes more hydrophilic (with contact angles closer to 120°), the increased wettability facilitates quicker droplet coalescence, resulting in shorter separation times. This phenomenon can be explained by the reduced resistance to interface merging at lower contact angles, which promotes faster droplet interactions and accelerates the separation process. As observed in the simulations, droplets on more hydrophilic surfaces have less resistance to forming a common interface, allowing for more efficient coalescence. The results of the single-objective optimization, based on different objective functions to determine the optimal initial contact angle for the model problem, are summarized in ▶**Table 1**. In this table, the objectives of minimizing droplet deformation and minimizing separation time are evaluated separately. Reducing separation time enhances efficiency, conserves energy, improves stability, and boosts performance across numerous engineering, industrial, and scientific fields. In systems where droplet dynamics play a critical role, achieving shorter separation times often leads to significant improvements in overall system performance. Conversely, minimizing droplet deformation is vital for maintaining the stability, efficiency, and accuracy of processes involving droplets. It allows for greater control over droplet behavior, resulting in more energy-efficient systems and better outcomes in applications ranging from microfluidics to printing technol-

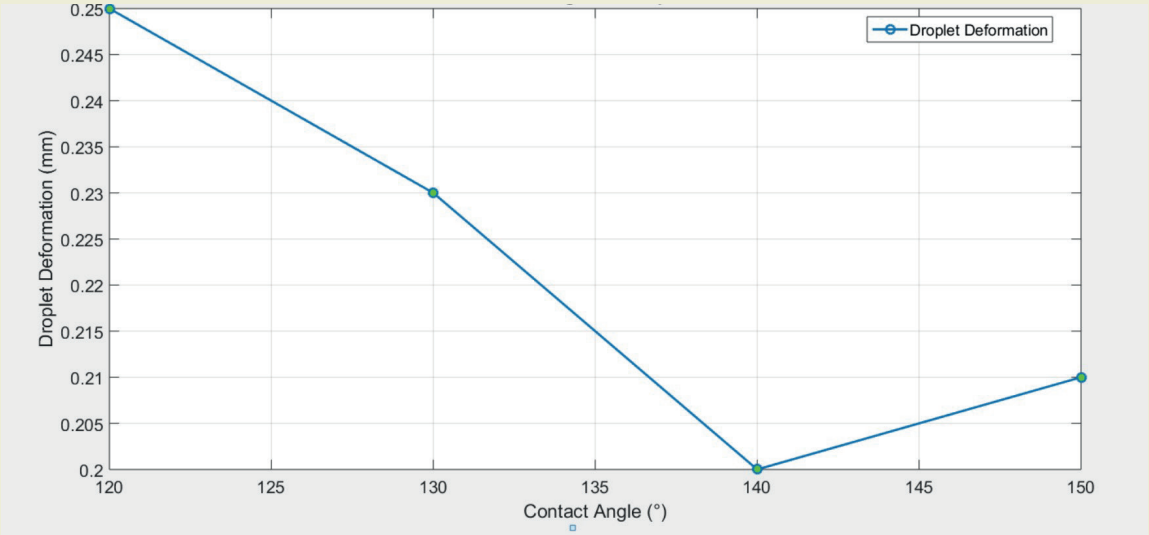

Figure 10. Effect of initial contact angle on droplet deformation.

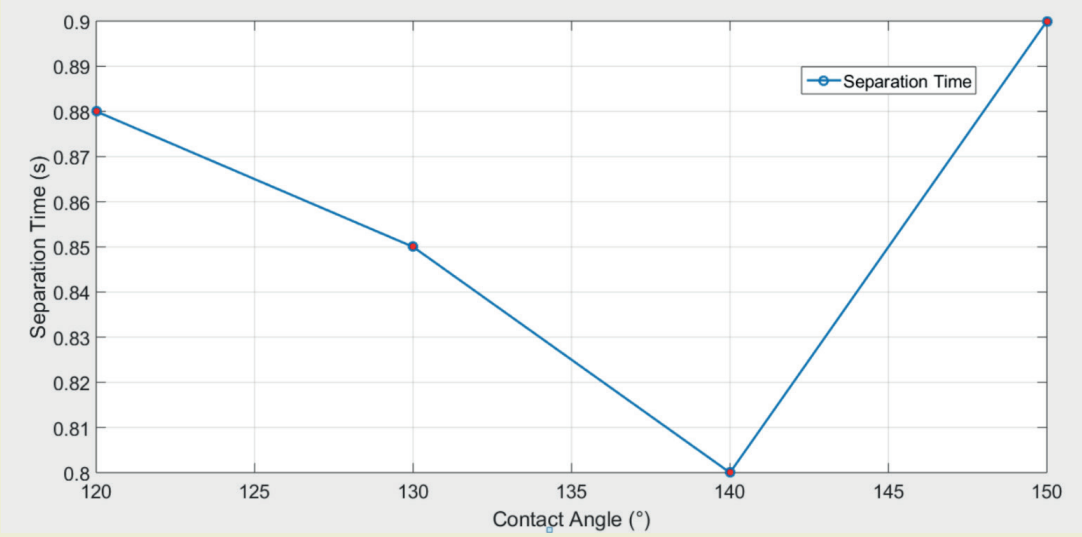

Figure 11. Effect of initial contact angle on droplet separation time.

ogies. By minimizing deformation, the droplet retains stability, structural integrity, and predictable responses to external forces, making it easier to manage and achieve desired results in various applications. For the objective of minimizing droplet deformation, the optimal initial contact angle was found to be 123.45° with a deformation value of 0.345 mm. This suggests that at this angle, the surface tension forces within the droplet are sufficient to counterbalance external forces, such as gravity or applied fields, that could otherwise deform it. This angle represents a stable equilibrium where the droplet maintains its shape, which is essential for ensuring proper functionality in applications such as material transport, micro-reactors in microfluidic systems, or precise deposition in printing and coating processes. For the objective of minimizing separation time, the optimal initial contact angle was determined to be 145.67° with a separation time of 1.23 seconds. This angle represents the point where the interaction between the droplet and the surface (or another droplet) is most conducive to rapid detachment. At this angle, surface tension forces are optimized for quick separation, and contact line dynamics favor rapid detachment. External forces, such as gravity or electric fields, are also more effective at facilitating separation at this contact

Table 1. Single objective optimization results for determination of optimum initial contact angle.

Objective function	Optimum initial contact angle (°)
Minimization of droplet deformation	123.45
Minimization of droplet separation time	145.67

angle. The optimization of droplet deformation and separation time revealed two competing objectives in this analysis. The multi-objective optimization, which focused on determining the ideal initial contact angle to balance these objectives, was conducted using the NSGA-II method. The resulting optimal Pareto frontier is shown in ▶**Figure 12**. To determine the best initial contact angle, equal weights (0.5) were assigned to both objective functions, and the TOPSIS method was applied. The results of the TOPSIS analysis are presented indicating that the optimal initial contact angle was 148°. Based on these optimization results, we conclude that if precision is the priority, as in printing technologies, biological experiments, or coating processes, the optimal contact angle of 123.45° should be selected for minimizing droplet deformation, as it maintains droplet shape with minimal distortion. If speed is the primary concern, as in spray drying, high-speed cooling, or large-scale manufacturing, the result focused on minimizing separation time (145.67°) will be more suitable, enabling faster droplet detachment and increased throughput. In systems that require a balance between these two objectives, such as biomedical applications, microfluidics, or complex multi-phase systems, the multi-objective optimization result of 148° offers a practical solution that balances both speed and precision, ensuring neither objective is overly compromised.

6. Conclusions

The contact angle was calculated for coalesced drop by following the contact line depending on time and plotting the contact angle variation against the applied electrical potential, which is compatible with Young-Lippmann law, and the dynamic variation of the contact angle against the Capillary number, which holds Cox-Voinov law, to check our solver with these two laws by choosing the proper applied electrical potential values. A comprehensive evaluation of the role of electrical forces in driving phase separation through electrocoalescence in laminar multiphase flows is provided in this study. The influence of varying electrical potentials on droplet behavior, interface dynamics, and separation efficiency was examined using a customized numerical solver that integrates the phase-field method with the Navier-Stokes equations. It was revealed through simulations that increasing the applied electrical potential from 50 kV to 100 kV significantly enhances phase separation efficiency, with the time required for complete separation being reduced by approximately 20%, from 0.15 seconds to 0.12 seconds. This improvement is attributed primarily to the stronger electrical forces, which induce greater droplet deformation, prevent the formation of stable liquid bridges, and promote quicker coalescence. Droplet deformation was quantified using the droplet deformation index (DDI), which was found to increase from 0.35 to 0.52 as the electrical potential was raised from 50 kV to 100 kV. This increase indicates a more pronounced asymmetric deformation of droplets, correlating with the observed acceleration in phase separation. A critical point was identified at an electrical potential of 80 kV, where droplet coalescence became more irregular, leading to the breakup of larger droplets into smaller ones, thereby further accelerating the separation process. Additionally, contact angle dynamics were monitored, and it was observed that contact angle hysteresis increased from 10° to 18° as the electrical potential was increased from 50 kV to 100 kV. This increase in hysteresis is indicative of more intense interactions between droplets and the solid surface under higher electrical fields, contributing to the observed changes in droplet behavior. The effectiveness of the numerical solver was validated through the quantitative data obtained from these simulations, which also provided new insights into the complex interactions between electrical forces and multiphase flow dynamics. These findings have significant implications for optimizing electrocoalescence processes in various industrial applications, such as oil-water separation, where precise control of phase separation is critical for operational efficiency. Future work will focus on the experimental validation of these numerical results and the exploration of the effects of non-uniform electric fields and more complex droplet configurations, with the aim of enhancing understanding and refining the numerical models used in electrocoalescence studies. In this study, the effects of varying the initial contact angle on the electrocoalescence process were investigated, with a focus on understanding how the contact angle influenced both droplet deformation and separation time. Additional simulations were conducted at contact angles of 120°, 130°, and 150° to provide a more comprehensive understanding of the relationship between surface wettability and droplet behavior. It was observed that increasing the contact angle led to more pronounced droplet deformation due to the increased hydrophobicity of the surface. This effect

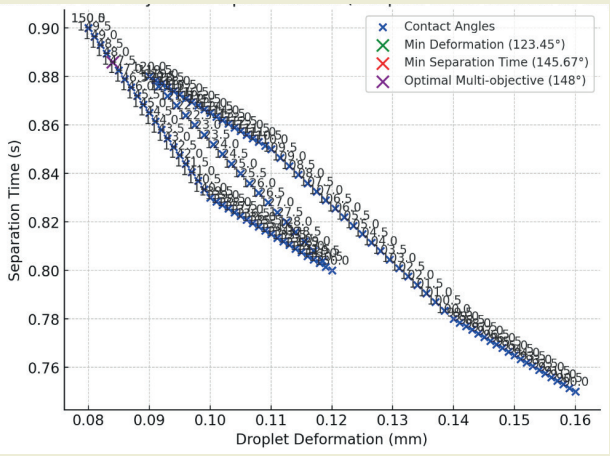

Figure 12. Pareto Frontier for multiobjective optimization of droplet deformation and separation time.

became more significant at contact angles above 140°, where the droplet exhibited greater instability at the interface. Lower contact angles promoted faster droplet coalescence, with shorter separation times observed at angles closer to 120°. The increased wettability at lower angles facilitated quicker droplet interactions and reduced resistance to merging. Through single and multi-objective optimizations, the ideal initial contact angles were determined based on the minimization of droplet deformation and separation time. The optimal initial contact angle was calculated to be 123.45°, with a deformation value of 0.345 mm. This angle represents the point where surface tension forces are sufficient to counter external forces, ensuring droplet stability and minimal deformation. The optimal initial contact angle was determined as 145.67°, with a separation time of 1.23 seconds, where the interaction between the droplet and surface optimizes rapid detachment. In balancing these conflicting objectives, a multi-objective optimization process using the NSGA-II method followed by the TOPSIS technique resulted in an optimal initial contact angle of 148°. This result offers a practical compromise between minimizing deformation and achieving efficient separation, making it suitable for applications where both speed and precision are necessary.

Nomenclature

Symbol Description

Bo	Bond number
Ca	Capillary number
Cn	Cahn number
DDI	Droplet Deformation Index
E	Electric field (V/m)
F_e	Electrical force (N)
F_s	Surface tension force (N)
H	Distance between plates (m)
κ	Curvature of the fluid-fluid interface (m^{-1})
μ	Dynamic viscosity (Pa·s)
p	Pressure (Pa)
Pe	Peclet number
ϕ	Phase-field variable
ρ	Density ($\mathrm{kg/m}^3$)
Re	Reynolds number
σ	Surface tension (N/m)
t	Time (s)
u	Velocity vector (m/s)
V_0	Applied voltage (V)
∇	Gradient operator
∇^2	Laplacian operator
We_{el}	Electrical Weber number
ϵ_0	Permittivity of free space (F/m)
ϵ_r	Relative permittivity of dielectric material

Research ethics

The study complies with research and publication ethics.

Author contributions

The author have accepted responsibility for the entire content of this manuscript and approved its submission.

Competing interests

The author states no conflict of interest.

Research funding

This research did not receive any specific grant from funding agencies in the public, commercial, or not-for-profit sectors.

Data availability

The raw data can be obtained on request from the corresponding author.

Peer-review

Externally peer-reviewed.

Orcid

Aslı Tiktaş https://orcid.org/0000-0003-3685-5134

References

[1] Eow, J. S., Ghadiri, M., & Sharif, A. O. (2002). Electrostatic and hydrodynamic separation of aqueous drops in a flowing viscous oil. *Chemical Engineering and Processing: Process Intensification, 41*(8), 649–657.

[2] Wu, J., Xu, Y., Dabros, T., & Hamza, H. (2003). Effect of demulsifier properties on destabilization of water-in-oil emulsion. *Energy & Fuels, 17*(6), 1554–1559.

[3] Dezhi, S., Chung, J. S., Xiaodong, D., & Ding, Z. (1999). Demulsification of water-in-oil emulsion by wetting coalescence materials in stirred-and packed-columns. *Colloids and Surfaces A: Physicochemical and Engineering Aspects, 150*(1–3), 69–75.

[4] Klasson, K. T., Taylor, P. A., Walker, J. F., Jr, Jones, S. A., Cummins, R. L., & Richardson, S. A. (2005). Modification of a centrifugal separator for in-well oil-water separation. *Separation Science and Technology, 40*(1–3), 453–462.

[5] Scalarone, D., & Chiantore, O. (2004). Separation techniques for the analysis of artists' acrylic emulsion paints. *Journal of Separation Science, 27*(4), 263–274.

[6] Pouliot, Y., Conway, V., & Leclerc, P. (2014). Separation and concent-

ration technologies in food processing. In *Food processing: Principles and applications* (pp. 33–60).

[7] Yesair, D. W., & Coutinho, C. B. (1970). Method for extraction and separation of drugs and metabolites from biological tissue. *Biochemical Pharmacology, 19*(5), 1569–1578.

[8] Abeynaike, A., Sederman, A. J., Khan, Y., Johns, M. L., Davidson, J. F., & Mackley, M. R. (2012). The experimental measurement and modelling of sedimentation and creaming for glycerol/biodiesel droplet dispersions. *Chemical Engineering Science, 79*, 125–137.

[9] Narváez-Muñoz, C., Hashemi, A. R., Hashemi, M. R., Segura, L. J., & Ryzhakov, P. B. (2024). Computational electrohydrodynamics in microsystems: A review of challenges and applications. *Archives of Computational Methods in Engineering*.

[10] Santra, S., Mandal, S., & Chakraborty, S. (2021). Phase-field modeling of multicomponent and multiphase flows in microfluidic systems: A review. *International Journal of Numerical Methods for Heat & Fluid Flow, 31*(10), 3089–3131.

[11] Li, J., Zheng, D., & Zhang, W. (2023). Advances of phase-field model in the numerical simulation of multiphase flows: A review. *Atmosphere, 14*(8), 1311.

[12] Abbasi, M. S., Song, R., Cho, S., & Lee, J. (2020). Electro-hydrodynamics of emulsion droplets: Physical insights to applications. *Micromachines, 11*(10), 942.

[13] Chen, L.-Q., & Zhao, Y. (2022). From classical thermodynamics to phase-field method. *Progress in Materials Science, 124*, 100868.

[14] Jain, S. S. (2022). Accurate conservative phase-field method for simulation of two-phase flows. *Journal of Computational Physics, 469*, 111529.

[15] Brenner, H. (2013). *Interfacial transport processes and rheology*. Elsevier.

[16] Sherwood, J. D. (1988). Breakup of fluid droplets in electric and magnetic fields. *Journal of Fluid Mechanics, 188*, 133–146.

[17] Cahn, J. W., & Hilliard, J. E. (1958). Free energy of a nonuniform system. I. Interfacial free energy. *Journal of Chemical Physics, 28*(2), 258–267.

[18] Probstein, R. F. (2005). *Physicochemical hydrodynamics: An introduction*. John Wiley & Sons.

[19] Krotov, V. V., & Rusanov, A. I. (1999). *Physicochemical hydrodynamics of capillary systems*. World Scientific.

[20] Lippmann, G. (1875). Démonstration élémentaire de la formule de Laplace. *Journal de Physique Théorique et Appliquée, 4*(1), 332–333.

[21] Dupré, A., & Dupre, P. (1969). *Théorie mécanique de la chaleur*. Gauthier-Villars.

[22] Li, X., Bodziony, F., Yin, M., Marschall, H., Berger, R., & Butt, H.-J. (2023). Kinetic drop friction. *Nature Communications, 14*(1), 4571.

[23] Butt, H.-J., et al. (2022). Contact angle hysteresis. *Current Opinion in Colloid & Interface Science, 59*, 101574.

[24] López-Herrera, J. M., Popinet, S., & Herrada, M. (2011). A charge-conservative approach for simulating electrohydrodynamic two-phase flows using volume-of-fluid. *Journal of Computational Physics, 230*(5), 1939–1955.

[25] Yang, Q., Li, B. Q., & Ding, Y. (2013). 3D phase field modeling of electrohydrodynamic multiphase flows. *International Journal of Multiphase Flow, 57*, 1–9.

[26] Fernandez, A., Tryggvason, G., Che, J., & Ceccio, S. L. (2005). The effects of electrostatic forces on the distribution of drops in a channel flow: Two-dimensional oblate drops. *Physics of Fluids, 17*(9).

[27] Maehlmann, S., & Papageorgiou, D. T. (2009). Numerical study of electric field effects on the deformation of two-dimensional liquid drops in simple shear flow at arbitrary Reynolds number. *Journal of Fluid Mechanics, 626*, 367–393.

[28] Lin, Y., Skjetne, P., & Carlson, A. (2012). A phase field model for multiphase electro-hydrodynamic flow. *International Journal of Multiphase Flow, 45*, 1–11.

[29] Hadidi, H., Kamali, R., & Manshadi, M. K. D. (2020). Numerical simulation of a novel non-uniform electric field design to enhance the electrocoalescence of droplets. *European Journal of Mechanics-B/Fluids, 80*, 206–215.

[30] Utiugov, G., Chirkov, V., & Reznikova, M. (2021). Application of the arbitrary Lagrangian-Eulerian method to simulate electrical coalescence and its experimental verification. *International Journal of Plasma Environmental Science & Technology, 15*.

[31] Sun, Z., Li, N., Li, W., Weng, S., Liu, T., & Wang, Z. (2024). Effect of droplet angle on droplet coalescence under high-frequency pulsed electric fields: Experiments and molecular dynamics simulations. *Chemical Engineering Science, 295*, 120195.

[32] Zhang, Z., Gao, M., Zhou, W., Wang, D., & Wang, Y. (2023). The numerical simulation of behaviors of oil-water-emulsion flow in pores by using phase field method. *Petroleum Science and Technology*.

[33] Alizadeh Majd, S., Moghimi Zand, M., Javidi, R., & Rahimian, M. H. (2023). Numerical investigation of electrohydrodynamic effect for size-tunable droplet formation in a flow-focusing microfluidic device. *Soft Materials, 21*(2), 174–190.

[34] Ou, G., Li, J., Jin, Y., & Chen, M. (2023). Droplet coalescence of W/O emulsions under an alternating current electric field. *Industrial & Engineering Chemistry Research, 62*(17), 6723–6733.

[35] Comsol. (2023). *IEEE Microwave Magazine, 24*(2). https://doi.org/10.1109/mmm.2022.3229860

[36] Kim, J. (2012). Phase-field models for multi-component fluid flows. *Communications in Computational Physics, 12*(3), 613–661.

[37] Jacqmin, D. (2000). Contact-line dynamics of a diffuse fluid interface. *Journal of Fluid Mechanics, 402*, 57–88.

[38] MathWorks. (2022). MATLAB (R2022a). The MathWorks Inc.

[39] Danish, M. (2022). Contact angle studies of hydrophobic and hydrophilic surfaces. In *Handbook of Magnetic Hybrid Nanoalloys and their Nanocomposites* (pp. 1–22). Springer.

[40] Zhu, Y., et al. (2023). Prediction of contact angle for oriented hydrophobic surface and experimental verification by micro-milling. *Coatings, 13*(8), 1305.

[41] Voinov, O. V. (1976). Hydrodynamics of wetting. *Fluid Dynamics, 11*(5), 714–721.

[42] Tiktaş, A., Gunerhan, H., & Hepbasli, A. (2023). Exergy and sustainability-based optimisation of flat plate solar collectors by using a novel mathematical model. *International Journal of Exergy, 42*(2), 192–215.